Relating Retinal Ganglion Cell Function and Retinal Nerve Fiber Layer (RNFL) Retardance to Progressive Loss of RNFL Thickness and Optic Nerve Axons in Experimental Glaucoma

Brad Fortune, Grant Cull, Juan Reynaud, Lin Wang, and Claude F. Burgoyne

Discoveries in Sight Research Laboratories, Devers Eye Institute and Legacy Research Institute, Legacy Health, Portland, Oregon, United States

Correspondence: Brad Fortune, Discoveries in Sight Research Laboratories, Devers Eye Institute and Legacy Research Institute, 1225 NE Second Avenue, Portland, OR 97232, USA; bfortune@deverseye.org.

Submitted: January 28, 2015
Accepted: April 29, 2015

Citation: Fortune B, Cull G, Reynaud J, Wang L, Burgoyne CF. Relating retinal ganglion cell function and retinal nerve fiber layer (RNFL) retardance to progressive loss of RNFL thickness and optic nerve axons in experimental glaucoma. *Invest Ophthalmol Vis Sci*. 2015;56:3936–3944. DOI:10.1167/iovs.15-16548

Purpose. To relate changes in retinal function and retinal nerve fiber layer (RNFL) retardance to loss of RNFL thickness and optic nerve axon counts in a nonhuman primate (NHP) model of experimental glaucoma (EG).

Methods. Bilateral longitudinal measurements of peripapillary RNFL thickness (spectral-domain optical coherence tomography, SDOCT; Spectralis), retardance (GDxVCC), and multifocal electroretinography (mfERG; VERIS) were performed in 39 NHP at baseline (BL; median, 5 recordings; range, 3–10) and weekly after induction of unilateral EG by laser photocoagulation of the trabecular meshwork. Multifocal ERG responses were high-pass filtered (>75 Hz) to measure high- and low-frequency component (HFC and LFC) amplitudes, including LFC features N1, P1, and N2. High-frequency component amplitudes are known to specifically reflect retinal ganglion cell (RGC) function. Complete (100%) axon counts of orbital optic nerves were obtained in 31/39 NHP.

Results. Postlaser follow-up was 10.4 ± 7.9 months; mean and peak IOP were 18 ± 5 and 41 ± 11 mm Hg in EG eyes, 11 ± 2 and 18 ± 6 mm Hg in control (CTL) eyes. At the final available time point, RNFL thickness had decreased from BL by 14 ± 14%, retardance by 20 ± 11%, and the mfERG HFC by 30 ± 17% ($P < 0.0001$ each). Longitudinal changes in retardance and HFC were linearly related to RNFL thickness change ($R^2 = 0.51$, $P < 0.0001$ and $R^2 = 0.22$, $P = 0.002$, respectively); LFC N2 was weakly related but N1 or P2 (N1: $R^2 = 0.07$, $P = 0.11$; P1: $R^2 = 0.04$, $P = 0.24$; N2: $R^2 = 0.13$, $P = 0.02$). At zero change from BL for RNFL thickness (*Y*-intercept), retardance was reduced by 11% (95% confidence interval [CI]: −15.3% to −6.8%) and HFC by 21.5% (95% CI: −28.7% to −14.3%). Relative loss of RNFL thickness, retardance, and HFC (EG:CTL) were each related to axon loss ($R^2 = 0.66$, $P < 0.0001$; $R^2 = 0.42$, $P < 0.0001$; $R^2 = 0.42$, $P < 0.0001$, respectively), but only retardance and HFC were significantly reduced at zero relative axon loss (*Y*-intercept; retardance: −9.4%, 95% CI: −15.5% to −3.4%; HFC: −10.9%, 95% CI: −18.6% to −3.2%; RNFL thickness: +1.8%, 95% CI: −4.9% to +5.4%).

Conclusions. Retinal nerve fiber layer retardance and RGC function exhibit progressive loss from baseline before any loss of RNFL thickness or orbital optic nerve axons occurs in NHP EG. These in vivo measures might serve as potential biomarkers of early-stage glaucomatous damage preceding axon loss and RGC death.

Keywords: glaucoma, axonal degeneration, ganglion cells, optical coherence tomography, scanning laser polarimetry

The retinal nerve fiber layer (RNFL) consists primarily of retinal ganglion cell (RGC) axons, which progressively degenerate in glaucoma, resulting in thinning and disappearance of axon bundles from the RNFL. Retinal nerve fiber layer defects may represent one of the earliest glaucomatous structural abnormalities manifest in clinical examination of the ocular fundus,[1–3] yet such defects can elude detection and are difficult to quantify by clinical examination or flash photography.[4,5] Advances in ophthalmic imaging technology such as scanning laser polarimetry (SLP)[6,7] and optical coherence tomography (OCT)[8] enable finer scrutiny and quantification of RNFL integrity. Indeed, the benefits of these imaging techniques have led to their rapid incorporation into the clinical regimen for glaucoma diagnosis and management, along with standard measures of vision function such as automated perimetry.[9–11] However, there are few studies that relate clinical surrogate measures such as RNFL thickness or retardance directly to histological measurements of RNFL thickness,[12–14] RGC soma counts,[15,16] or optic nerve axon counts.[17–19] Therefore the first purpose of the present study was to compare the magnitude of longitudinal change for in vivo measurements of RNFL thickness, retardance, and specific

measures of RGC function to the magnitude of RGC axon loss obtained by complete (100%) postmortem counts of each orbital optic nerve in a nonhuman primate (NHP) model of experimental glaucoma (EG).

The second purpose of the present study was to perform a cross-sectional analysis of the same longitudinal data in order to compare the relative degree of change measured by each in vivo measure. Specifically, it is thought that RNFL retardance measured by SLP reflects the integrity of axonal cytoskeletal ultrastructure,[20–24] which might become disrupted prior to axon loss and bundle thinning and thus represent an important biomarker of early-stage injury.[21,25] We have tested this hypothesis previously in two different ways using longitudinal data from NHP EG. In the first of these studies, we found that RNFL retardance alterations measured by SLP and RGC functional loss measured specifically by multifocal electroretinography (mfERG) were present at (or before) the onset of posterior deformation of the optic nerve head (ONH) surface and prior to thinning of the peripapillary RNFL measured by spectral-domain OCT (SDOCT).[26] In a subsequent study, we found that the onset of RNFL retardance alterations preceded the onset of RNFL thinning in ~80% of EG eyes and with a lead time of ~3 months.[27] Here we extend the test of this hypothesis by comparing the magnitude of longitudinal change for RNFL retardance and RGC function to the magnitude of longitudinal RNFL thickness change at the final available time point (when axon counts are also obtained).

Methods

Subjects

The subjects of this study were 39 rhesus macaque monkeys (*Macaca mulatta*), 31 female and 8 male. At the start of study, their average age (± standard deviation, SD) was 9.9 ± 6.8 years, ranging from 1.4 to 22.6 years; weight was 5.7 ± 1.3 kg (range, 3.3–8.9 kg). This study was carried out in strict accordance with the recommendations in the Guide for the Care and Use of Laboratory Animals of the National Institutes of Health and were approved and monitored by the Institutional Animal Care and Use Committee (IACUC) at Legacy Health (USDA license 92-R-0002 and OLAW assurance A3234-01). All experimental methods and animal care procedures also adhered to the ARVO Statement for the Use of Animals in Ophthalmic and Vision Research.

Anesthesia

All experimental procedures began with induction of general anesthesia using ketamine (10–25 mg/kg intramuscular [IM]) in combination with either xylazine (0.8–1.5 mg/kg IM) or midazolam (0.2 mg/kg [IM]), along with a single injection of atropine sulphate (0.05 mg/kg IM). Animals were then intubated with an endotracheal tube to breathe a mixture of 100% oxygen and air for maintaining oxyhemoglobin saturation ≥ 95%, as close to 100% as possible. During ERG retinal function testing, anesthesia was maintained using a combination of ketamine (5 mg/kg/h intravenous [IV]) and xylazine (0.8 mg/kg/h IM). In some cases, a constant rate infusion (1.2–3.0 mg/kg/h) was used for IV ketamine delivery after a loading dose of 3.0 to 8.0 mg/kg. Upon completion of ERG testing, ketamine-xylazine administration was discontinued, and isoflurane gas (1%–2%) was mixed with oxygen to provide anesthesia during SLP scan acquisition. For all SDOCT imaging sessions, anesthesia after initial induction was maintained using isoflurane gas (1%–2%; typically 1.25%) mixed with 100% oxygen and delivered via endotracheal tube. For SLP and SDOCT imaging, a clear, rigid gas-permeable contact lens filled with 0.5% carboxymethylcellulose solution was placed over the apex of each cornea. In all sessions, IV fluids (lactated Ringer's solution, 10–20 mL/kg/h) were administered via the saphenous vein. Vital signs were monitored throughout and recorded every 10 to 15 minutes, including heart rate, blood pressure, arterial oxyhemoglobin saturation, end-tidal CO_2, and body temperature; body temperature was maintained at 37°C, heart rate above 75 per minute, and oxygen saturation above 95%.

SDOCT Measurements of Peripapillary RNFL Thickness

Peripapillary RNFL thickness was measured using SDOCT (Spectralis; Heidelberg Engineering GmbH, Heidelberg, Germany).[19,26–28] For this study, the average peripapillary RNFL thickness was measured from a single circular B-scan consisting of 1536 A-scans. Nine to sixteen individual sweeps were averaged in real time to comprise the final stored B-scan at each session. The position of the scan was centered on the ONH at the first imaging session, and all follow-up scans were acquired at this same location using the instrument's automatic active eye-tracking software. A trained technician masked to the purpose of this study manually corrected the accuracy of the instrument's native automated layer segmentations when the algorithm had obviously erred from the inner and outer borders of the RNFL to an adjacent layer (such as a refractive element in the vitreous instead of the internal limiting membrane, or to the outer border of the inner plexiform layer instead of the RNFL). All SDOCT scans were performed 30 minutes after intraocular pressure (IOP) was manometrically stabilized to 10 mm Hg.

SLP Measurements of Peripapillary RNFL Retardance

Peripapillary RNFL retardance measurements were obtained by SLP using a GDxVCC instrument (Carl Zeiss Meditec, Inc., Dublin, CA, USA).[23,25–27,29] Three RNFL scans were averaged for each eye at each time point. Values of RNFL retardance were exported for the "small" peripapillary locus, which is an 8-pixel-wide band centered on the optic disc with a mean scan radius of 4.84°,[30] corresponding to approximately 1.2 mm on the macaque retina. The average of the 64 exported peripapillary samples was taken as the summary parameter for each eye and time point. All SLP scans were performed at the end of the retinal function testing session without manometric IOP control since cannulation of the anterior chamber would interfere with ERG recordings. Since SLP scans are acquired after ~2 hours of ketamine/xylazine anesthesia, IOP is always low (near 10 mm Hg) in both eyes, including EG eyes whose ambient IOP was elevated at the start of the session. The IOP reduction begins within minutes of anesthesia induction. We have documented that IOP elevation does not exert any meaningful influence on RNFL thickness or retardance as measured in this study.[29] We have also previously performed the inverse experiment whereby IOP is manometrically lowered from a chronically elevated level in EG eyes (~30 mm Hg, $n = 3$), and the results similarly show no effect on peripapillary RNFL thickness or retardance measurements (structural changes are limited to within the area of the ONH, data not published).

Multifocal ERG Measurements of Retinal Function

Retinal function was evaluated by mfERG.[25,26,31,32] Briefly, mfERGs were recorded using VERIS (Electro-Diagnostic Imag-

Investigative Ophthalmology & Visual Science

ing, Inc., Redwood City, CA, USA). The mfERG stimulus consisted of 103 unscaled hexagonal elements subtending a total field size of ~55°. The luminance of each hexagon was independently modulated between dark (1 cd/m^2) and light (200 cd/m^2) according to a pseudorandom, binary m-sequence. The temporal stimulation rate was slowed by insertion of seven dark frames into each m-sequence step ("7F"). The m-sequence exponent was set to 12; thus the total duration of each recording was 7 minutes and 17 seconds. Signals were amplified (gain = 100,000), band-pass filtered (10–300 Hz; with an additional 60-Hz line filter), sampled at 1.2 kHz (i.e., sampling interval = 0.83 ms), and digitally stored for subsequent offline analyses. Two such recordings were obtained for each eye at each time point and averaged.

From the average of the two recordings at each time point, a subset of local responses from the full array, limited to the central element and the three rings surrounding it (37 local responses in total), was processed to derive summary outcome parameters. A high-pass filter (5-pole, >75 Hz) was applied to each local mfERG response to extract the high-frequency components (HFC). The low-frequency component (LFC) of each response was represented as the raw response minus the HFC. The amplitude of the HFC was calculated as the root mean square (RMS) for the epoch between 0 and 80 ms of each filtered record. Peak amplitudes for LFC features were quantified as follows: The first negative feature (N1) was calculated as the maximum negative excursion from baseline in the epoch up to 30 ms; the amplitude of the first positivity (P1) was calculated as the voltage difference between the maximum peak and the N1 trough; and the second negativity (N2) was calculated as the difference between baseline and the minima from 30 to 80 ms. The global average (of 37 response locations) for each parameter represented the measurement for each eye at each ERG session.

Intraocular Pressure Measurements

Intraocular pressure was measured in both eyes at the start of every session using a Tonopen XL (Reichert Technologies, Inc., Depew, NY, USA). The value recorded for each eye was the average of three successive measurements.

Experimental Design and Protocol

Each animal had a minimum of three weekly baseline recordings for each of the above-described imaging sessions (median number of prelaser baseline sessions, 5; range, 3–10). Argon laser photocoagulation was then applied to the trabecular meshwork of one eye of each animal to induce chronic elevation of IOP.[33,34] Initially, 180° of the trabecular meshwork was treated in one session; then the remaining 180° was treated in a second session approximately 2 weeks later. If necessary, laser treatments were repeated in subsequent weeks (limited to a 90° sector) until an IOP elevation was first noted or if the initial postlaser IOP had returned to normal levels. The average number of laser treatments (±SD) was 5.6 ± 2.5.

After initiation of laser photocoagulation, the type of testing alternated weekly between SDOCT imaging one week and mfERG+SLP the next week. Testing continued for each animal until its predefined sacrifice target had been reached. Specific targets for the EG stage when each animal was sacrificed were based on the primary study to which each animal was assigned and were predetermined based on those protocols. Thus the EG stage at sacrifice and details of sacrifice procedures differed across animals, providing a relatively wide range of damage for the cross-sectional analysis in this study. In all cases, death occurred by exsanguination under deep anesthesia (overdose of pentobarbital in $n = 19$ and under deep isoflurane anesthesia in $n = 20$). Optic nerve tissue was obtained for axon counts as described in the next section.

Optic Nerve Axon Counts

Optic nerve tissue samples were available for 31 of the 39 animals in this study (tissues for the other 8 were used in other studies and unavailable for axon counts). This group of 31 animals had an average age at death of 12.0 ± 7.5 years, ranging from 2.7 to 26.1 years. Complete (100%) axon counts were obtained from the retrobulbar optic nerve.[18,19,35,36] Tissues were preserved by perfusion fixation with either 4% paraformaldehyde ($n = 19$) or 4% paraformaldehyde followed by 5% gluteraldehyde ($n = 12$). A 2- to 3-mm sample of each optic nerve, beginning 2 mm posterior to the globe, was cut with a vibrotome (VT 100S; Leica Microsystems GmbH, Wetzlar, Germany) into 0.5-mm-thick transverse sections. Each of these thick optic nerve sections was postfixed in 4% osmium tetroxide and embedded in epoxy resin. Optic nerve cross sections (1 μm thick) were then cut and stained with p-phenylenediamine and mounted on glass slides. The most complete and uniformly stained section from each optic nerve was then chosen for axon counting. Images covering 100% of the optic nerve cross section were automatically captured using an inverted light microscope (DM IRB; Leica Microsystems GmbH) with an oil immersion ×100 objective (PL Fluotar NA = 1.3; Leica Microsystems GmbH) and custom software for X-Y-Z stage control (Applied Scientific Instrumentation, Inc., Eugene, OR, USA) and image capture. Automated axon counting software[35] was used to count all of the axons with normal morphological characteristics in each optic nerve cross section. The total axon count for each optic nerve was represented by the sum of all counted axons across all images tiling its entire cross sectional area; axons falling within the 15%-overlap area between adjacent tiles were counted only once.

Analysis and Statistics

The final measurement of RNFL thickness was tabulated for all 39 animals. In 5 of the 39, the final SLP/mfERG measurement occurred after the final RNFL thickness measurement (by 6.2 ± 1.3 days); so in order to maintain a conservative comparison, in these 5 animals the SLP/mfERG measurements were taken from the next nearest session prior to the final RNFL thickness measurement. Thus, across the entire group of $n = 39$, the time from the final SLP/mfERG measurement to the final RNFL thickness measurement ranged from zero to 21 days (average ± SD: 9.1 ± 4.9 days, median of 7 days; 85% were <14 days; one animal had all tests done on the same final session). In order to characterize the magnitude of longitudinal change in each eye, the difference between the value of the final measurement and the average of all baseline measurements was expressed as a fraction of the baseline average. A cross-sectional analysis ($n = 39$) was applied to relate the magnitude of longitudinal change of RNFL retardance and retinal function to the magnitude of longitudinal change of RNFL thickness using paired *t*-tests and linear regression. Since there are no longitudinal data for axon counts, comparisons of the magnitude of change between in vivo data and axon counts were performed using the ratio of the value in the EG eye to the fellow control eye for each animal ($n = 31$). Note that for those comparisons, the absolute final available data were used; thus in the 5 animals whose final SLP/mfERG session was ~1 week later than the final RNFL thickness measurement, the SLP/mfERG data differ slightly from those used strictly for comparison among in vivo measures. In the group of $n = 31$ animals with axon counts, the time between final RNFL

Investigative Ophthalmology & Visual Science

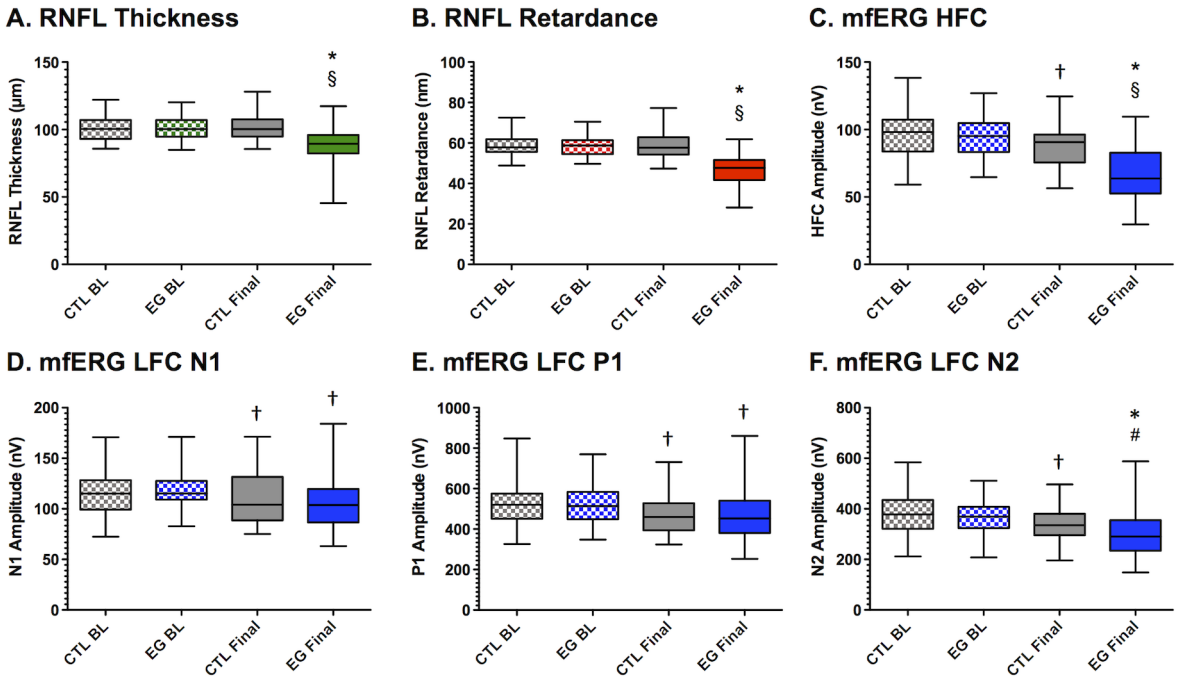

Figure 1. Longitudinal data for in vivo parameters. Box plots represent the distribution (median, interquartile range, and extremes; $n = 39$ NHP) of each in vivo parameter measured in control (CTL) and experimental glaucoma (EG) eyes at baseline (BL) and at the final time point. *$P < 0.0001$ versus BL; †$P < 0.01$ versus BL; §$P < 0.0001$ versus CTL eye group at final time point; #$P < 0.01$ versus CTL eye group at final time point.

thickness measurement and euthanasia ranged from 0 to 11 days (average ± SD: 4 ± 3.2 days). All statistical analysis was performed using a commercial software package (Prism 5; GraphPad Software, Inc., La Jolla, CA, USA).

Results

The average duration of postlaser follow-up (±SD) was 10.4 ± 7.9 months (range, 2.0–36.9 months). Mean IOP over the span of postlaser follow-up ranged from 10.4 to 29.4 mm Hg in the group of 39 EG eyes, with a group average of 18.3 ± 5.1 mm Hg. Mean IOP in the group of 39 fellow control eyes was 11.0 ± 2.0 mm Hg. The peak IOP observed during the postlaser follow-up period was 41.1 ± 11.2 in the EG eyes (range, 15.3–60.3 mm Hg) and 17.9 ± 6.4 mm Hg in control eyes.

The magnitude of RNFL thickness at baseline was 101.1 ± 9.4 µm and 101.2 ± 9.8, respectively, in the group of eyes assigned to be EG and fellow control eyes ($P = 0.80$). At the final available time point, RNFL thickness had declined to 86.7 ± 15.1 µm in EG eyes ($P < 0.0001$) but had not changed in fellow control eyes (101.9 ± 10.9, $P = 0.20$, Fig. 1A). Retinal nerve fiber layer retardance at baseline was 58.5 ± 5.2 µm and 58.6 ± 5.2, respectively, in the group of eyes assigned to be EG and fellow control eyes ($P = 0.92$). At the final available time point, RNFL retardance had declined to 46.6 ± 7.2 µm in EG eyes ($P < 0.0001$) but had not changed in fellow control eyes (58.9 ± 6.3, $P = 0.50$, Fig. 1B). The mfERG HFC amplitude at baseline was 94.8 ± 15.4 nV and 96.3 ± 16.8 nV, respectively, in the group of eyes assigned to be EG and fellow control eyes ($P = 0.13$). At the final available time point, mfERG HFC amplitude had declined to 66.8 ± 19.3 nV in EG eyes ($P < 0.0001$) and also declined slightly in fellow control eyes (to 87.8 ± 15.8 nV, $P = 0.0001$, Fig. 1C). The average change from baseline in EG eyes was −14.1 ± 14.1% for RNFL thickness (range, +8.8% to −52.1%), −20.2 ± 11.2% for RNFL retardance (range, −4.4% to −44.1%), and −29.7 ± 16.6% for mfERG HFC amplitude (range, +10.4% to −54.4%). The decline in the control eye group for mfERG HFC amplitude represented a −8.2 ± 12.2% change from their baseline amplitudes. The amplitudes of the mfERG LFC features also declined slightly from baseline in both EG and fellow control eye groups: N1 decreased by 10.3 ± 16.7% and 4.8 ± 16.3% in EG and control eyes, respectively, but there was no significant difference in the magnitude of change between EG and control eyes ($P = 0.10$, Fig. 1D); P1 decreased by 9.0 ± 17.1% and 8.5 ± 12.0% in EG and control eyes, respectively, but again there was no significant difference in the magnitude of change between EG and control eyes ($P = 0.88$, Fig. 1E); N2 decreased by 19.4 ± 17.8% and 9.5 ± 13.7% in EG and control eyes, respectively, a difference that was greater in EG as compared to control eyes ($P = 0.006$, Fig. 1F). The longitudinal changes observed in the fellow control eye group for all mfERG parameters suggest possible effects of chronic exposure to anesthesia, frequency of the testing protocol, and perhaps aging, which appear to impact EG and control eyes equally for the LFC features N1 and P1.

Retinal nerve fiber layer thickness was inversely correlated with age at baseline in the group of eyes assigned to have EG ($R = -0.45$, $P = 0.004$) and in the group of fellow control eyes ($R = -0.53$, $P = 0.001$).[19] The RNFL thickness was also inversely correlated with age at the final time point in the control eyes ($R = -0.49$, $P = 0.002$), but not significantly in the EG eyes ($R = -0.26$, $P = 0.11$). The magnitude of RNFL thickness longitudinal change in EG eyes (from baseline to final time point) was unrelated to age ($R = 0.03$, $P = 0.84$), however, it was correlated with mean IOP ($R = -0.55$, $P = 0.0003$), peak IOP ($R = -0.60$, $P < 0.0001$), and cumulative intereye IOP difference ($R = -0.49$, $P = 0.001$). When age was included with IOP factors in a multivariate analysis without an interaction term, age was not a significant predictor of RNFL thickness loss in EG eyes ($P = 0.52$ for a model based on age and mean IOP; $P = 0.88$ for a model based on age and peak IOP). Inclusion of an interaction term between age and IOP produced a worse

Investigative Ophthalmology & Visual Science

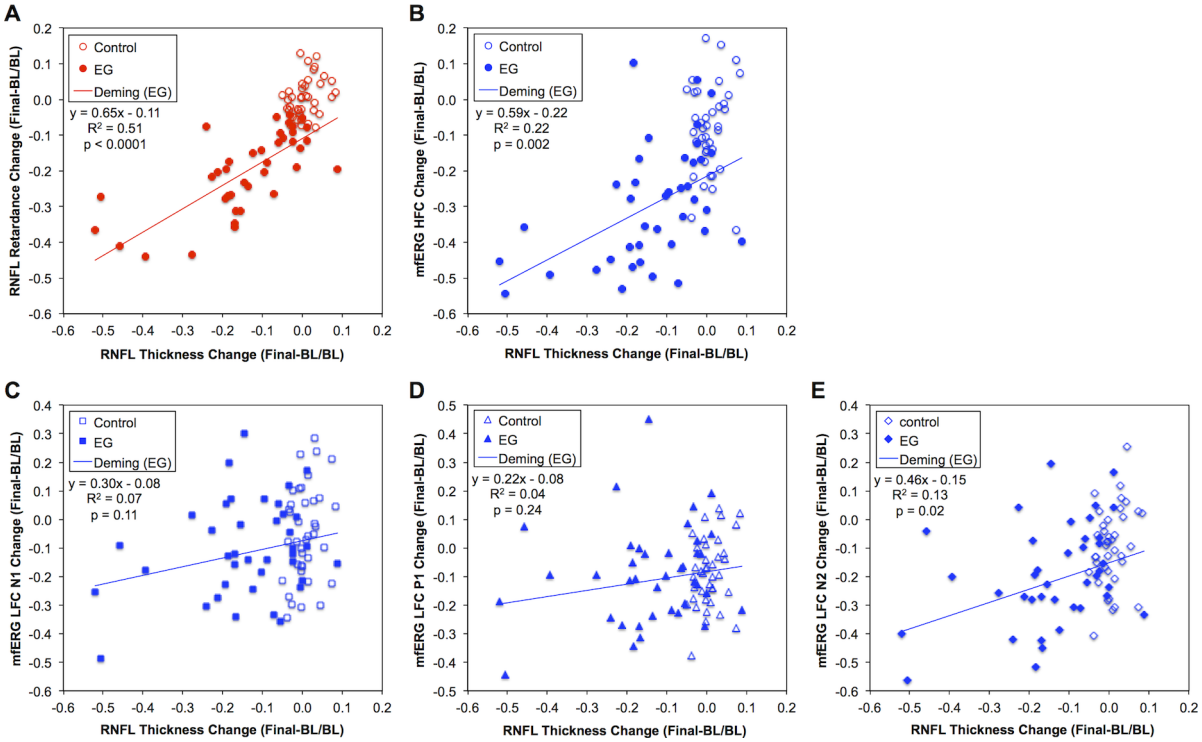

Figure 2. Comparison of longitudinal change from baseline to the final time point across in vivo parameters. Relative change from baseline in each eye was measured as the difference between the value of the final measurement and the average of all baseline measurements expressed as a fraction of the baseline average. Scatter plots show the change in RNFL retardance (**A**), mfERG HFC amplitude (**B**), mfERG LFC N1 amplitude (**C**), mfERG LFC P1 amplitude (**D**), and mfERG LFC N2 amplitude (**E**) against the change in RNFL thickness. *Solid lines* through EG data of each figure part and the equation in the legend represent the result of Deming regression (though note that R^2 values were obtained by ordinary least squares regression [OLSR]).

model (lower R^2) with no significant coefficients (masking the significant effect of IOP in both cases, mean or peak IOP).

Neither age nor IOP was a significant predictor of axon loss in EG eyes (axon count relative to control eye) in univariate or multivariate analyses; for the latter, there was also no significant interaction between age and mean IOP ($P = 0.15$) or between age and peak IOP ($P = 0.59$). Note that there were eight fewer data points for the model to predict axon loss, so the power to detect significant interactions between age and IOP may have been limited (and was not a goal of this study).

One main purpose of this study was to relate the magnitude of longitudinal change from baseline to the final time point for RNFL retardance and retinal function to the same measure of change for RNFL thickness. The results of this analysis are presented in Figure 2. The magnitude of longitudinal change in RNFL retardance was linearly related to RNFL thickness change in EG eyes (Fig. 2A). Importantly, however, the *Y*-intercept of this function was significantly below zero (−12.2%; 95% confidence interval, CI: −15.9% to −8.5%). The inference drawn from this result is that the SLP measure of RNFL retardance exhibits damage before any measurable change in RNFL thickness occurs (i.e., at zero relative change from baseline). This result is reinforced by the clear vertical separation of EG and fellow control eyes within the range of measurement noise for RNFL thickness (i.e., within ±7% of zero along the abscissa). Since the independent variable in this case also has inherent error, Deming regression was applied to confirm that the *Y*-intercept was negative and did not include zero (−11.0%; 95% CI: −15.3% to −6.8%).

Similar results were observed for the mfERG HFC amplitude (Fig. 2B), which was also linearly related to RNFL thickness change and exhibited a *Y*-intercept that was significantly below zero (−21.9%; 95% CI: −28.7% to −15.0%) in EG eyes. The inference drawn from this result is that RGC function as measured by the mfERG HFC amplitude is also reduced before any measurable change in RNFL thickness occurs, notwithstanding that measurement noise for mfERG HFC (±33%) is higher than that for RNFL retardance (±10%) or RNFL thickness (±7%) as determined by bootstrapping analysis of baseline data series.[27,28] Again, given that the independent variable has inherent error, Deming regression was applied to confirm that the *Y*-intercept was negative and did not include zero (−21.5%; 95% CI: −28.7% to −14.3%).

Relative amplitudes of the mfERG LFC features N1 and P1 were not related to RNFL thickness change (Figs. 2C, 2D, respectively) in EG eyes, nor was there any significant separation from the magnitude of change observed in the fellow control eye group (refer also to Figs. 1D, 1E). In contrast, longitudinal change in amplitude of the mfERG LFC feature N2 did exhibit a modest linear relationship to RNFL thickness change (Fig. 2E) and a small but significant difference from the changes observed in control eyes (Fig. 1F). These results suggest that the LFC feature N2 may also reflect RGC function in progressive EG, albeit to a lesser extent than does the HFC amplitude. Other investigators have suggested that the N2 feature of mfERG responses to slow-sequence stimulation may be homologous to the photopic negative response (PhNR) of the full-field flash ERG (Viswanathan S, et al. *IOVS* 2009;50:ARVO E-Abstract 4758),[37] which is well documented to be altered in both EG models and human glaucoma.[38–42]

The second main purpose of this study was to relate the in vivo measurements of RNFL structure and retinal function to postmortem orbital optic nerve axon counts. The magnitude of RNFL thickness loss was linearly related to the degree of

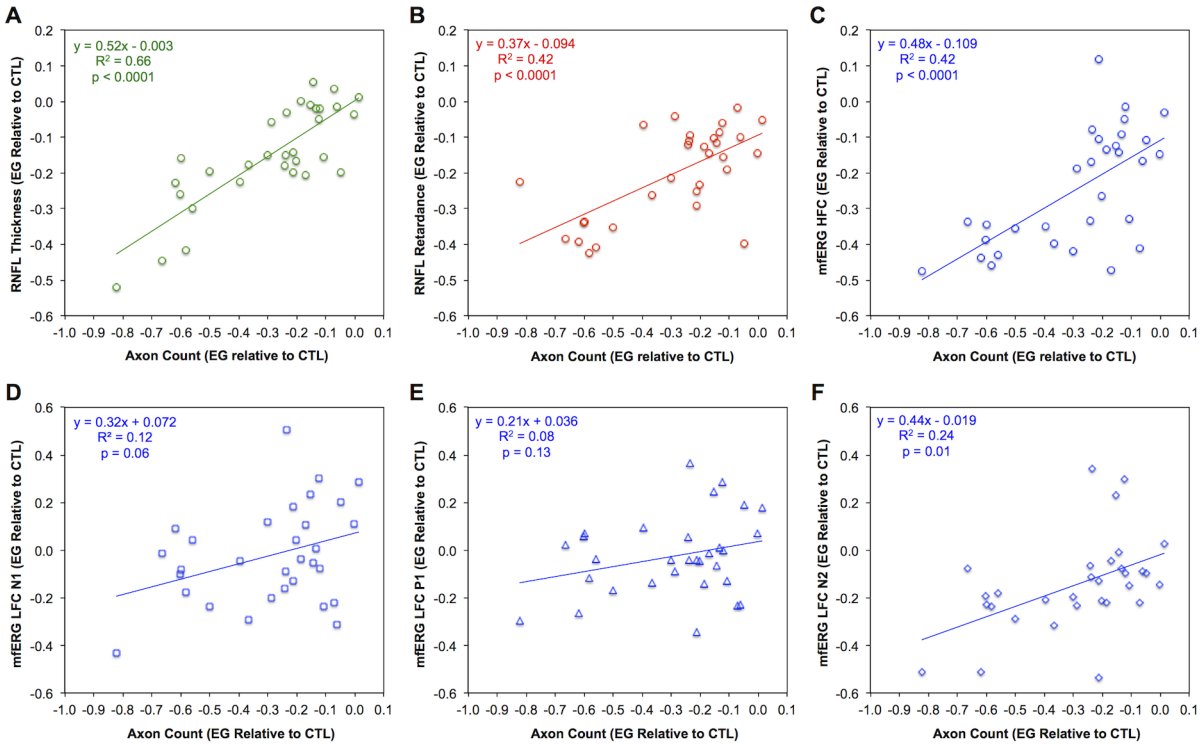

Figure 3. Comparison of in vivo parameter changes at the final time point to postmortem optic nerve axon counts. Relative loss for each parameter was measured as the difference between the final value recorded in each EG eye and the value recorded in the fellow control eye at the same time point, expressed here as a fraction of the control eye value. Scatter plots show the relative loss for RNFL thickness (**A**), RNFL retardance (**B**), mfERG HFC amplitude (**C**), mfERG LFC N1 amplitude (**D**), mfERG LFC P1 amplitude (**E**), and mfERG LFC N2 amplitude (**F**) against the relative loss of optic nerve axons in each eye; $n = 31$. *Solid lines* in each figure part represent result of Deming regression (equation is shown in the legend, though note that R^2 values were obtained by OLSR).

damage measured by axon counts (Fig. 3A). The magnitudes of RNFL retardance loss (Fig. 3B) and RGC functional loss (mfERG HFC amplitude, Fig. 3C) were also both related to axon loss. However, the *Y*-intercept (i.e., the magnitude of in vivo parameter change associated with zero axon loss) differed significantly among these three measures ($F_{2,87} = 3.7$, $P = 0.03$). The *Y*-intercept was significantly below zero for both RNFL retardance (−9.5%, 95% CI: −15.5% to −3.6%) and mfERG HFC amplitude (−10.9%, 95% CI: −18.6% to −3.2%), but was not significantly different from zero for RNFL thickness (+0.1%, 95% CI: −5.0% to +5.2%). The inference drawn from these results is that RNFL retardance loss as measured by SLP and RGC functional loss as measured by mfERG HFC amplitude occur before any difference can be measured in orbital optic nerve axon counts. Deming regression was applied in all three cases to confirm the results for the *Y*-intercept (at zero axon loss): The *Y*-intercept was negative and did not include zero for RNFL retardance (−9.4%; 95% CI: −15.5% to −3.4%) or mfERG HFC (−10.9%; 95% CI: −18.6% to −3.2%), but was not different from zero for RNFL thickness (+1.8%; 95% CI: −4.9% to +5.4%). The data plotted in Figures 3D and 3E show that changes in mfERG LFC features N1 and P1, respectively, were not significantly related to optic nerve axon loss, while Figure 3F shows that the magnitude of change for mfERG LFC feature N2 was only weakly related to axon loss in EG. None of these three functions relating mfERG LFC amplitude changes to axon loss had an intercept that was significantly different from zero.

Discussion

In this study we applied cross-sectional analyses to compare longitudinal in vivo measurements of RNFL retardance and retinal function to RNFL thickness and to compare all three in vivo measures to postmortem optic nerve axon counts in a NHP model of EG. We found that both RNFL retardance as measured by SLP and RGC function as measured by mfERG HFC amplitudes exhibit progressive loss from baseline before any loss of RNFL thickness or orbital optic nerve axons occurs. This suggests that both in vivo measures are detecting alterations that precede axon loss: cytoskeletal disruption within RGC axons in the case of RNFL retardance and RGC functional loss in the case of mfERG HFC amplitudes. These measures might thus serve as potential biomarkers of early-stage glaucomatous damage that precede axon loss and RGC death. We hope to conduct future studies designed to test whether this early damage stage is reversible with therapeutic intervention.

One limitation of this study is that it is based on cross-sectional analysis. This was necessary in order to compare the in vivo measurements to postmortem orbital optic nerve axon counts (which are not yet obtainable as a longitudinal in vivo measurement). We have previously applied longitudinal analyses and found similarly that RNFL retardance changes and RGC functional loss precede RNFL thickness loss during the early stages of progressive damage in this model.[26,27] We have also shown by similar analyses of longitudinal data that posterior deformation of the ONH surface as measured using confocal scanning laser tomography precedes RNFL thickness loss in this NHP EG model.[26,28,43–45] Further, we have reported results of several studies showing that deeper changes to structures beneath the ONH surface detectable by SDOCT imaging also precede RNFL thickness loss (as well as RNFL retardance and RGC functional changes).[43–45] Collectively, these results suggest a sequence of damage in this NHP EG

model whereby chronic mild-to-moderate IOP elevation results in deformation of ONH subsurface structures, subsequent injury to RGCs characterized by RNFL retardance (disruption of the axonal cytoskeleton), and RGC functional loss, with eventual RGC death, axon loss, and thinning of the peripapillary RNFL. Though commonly used as a measure of structural integrity in the clinical management of glaucoma, our data indicate that RNFL thinning is a relatively late event in the pathogenesis of glaucomatous damage, quite possibly too late (at least until it becomes possible to regenerate axons from the eye and establish correct synaptic connections at their central target).[46]

Another limitation of this study relates to the in vivo testing protocol in which the SLP/ERG tests and the SDOCT imaging (to obtain RNFL thickness measures) are performed in alternating weekly sessions throughout the course of postlaser follow-up. Testing sessions would be too long for animal welfare concerns if all tests were combined into any single imaging session. We attempted to mitigate any risk of bias against our null hypothesis by selecting in all 39 animals the SLP/ERG session from the session (~1 week) prior to the final available SDOCT session (RNFL thickness measurement). Thus if damage continued to progress, we would not be comparing a later time point for SLP/ERG to the final available RNFL thickness measurement (a risk otherwise relevant to 5 of the 39 animals).

A third limitation of this study is that none of the measurements are age corrected. If aging changes have a greater effect on SLP measurements of RNFL retardance or mfERG measurements of retinal function than they do on RNFL thickness measurements, this could confound our hypothesis test based on comparison of longitudinal changes. Data from the fellow control eye group showed little or no aging effect for either RNFL retardance or thickness over the duration of this study. However, we did find a significant change from baseline in both EG and fellow control eyes for all mfERG parameters, which may include possible effects of chronic exposure to anesthesia, frequency of the testing protocol, and perhaps aging. Nevertheless, the longitudinal changes observed in the glaucomatous eyes for the HFC amplitudes far exceeded changes in control eyes, whereas there were little or no differences observed between EG and fellow control eyes for longitudinal changes in the LFC features N1 or P1. Similarly, N1 and P1 were unrelated to axon loss across a wide range of damage (Fig. 3). These results are consistent with the interpretation that the HFC of mfERG responses to slow-sequence stimulation represent RGC function specifically, while the LFC features N1 and P1 reflect predominantly the function of retinal neurons distal to RGCs.[25,31,32,37,47] Interestingly, the results reported here reveal that the LFC feature N2, in contrast to its N1 and P1 counterparts, is specifically affected by EG (Fig. 1F) and exhibits a modest relationship to both progressive loss of RNFL thickness (Fig. 2E) and optic nerve axon loss (Fig. 3F). These findings for LFC N2 were not as strong as those observed for the mfERG HFC, but they suggest that RGC function manifests to some degree in the LFC feature N2, not solely in the HFC. Other investigators have reported evidence suggesting that some portion of slow-sequence mfERG LFC is RGC dependent[37] and that the N2 feature in particular may be the mfERG homologue of the full-field ERG PhNR (Viswanathan S, et al. *IOVS* 2009;50:ARVO E-Abstract 4758).[38,39,41] This might explain our findings for N2 in this study.

Finally, a fourth limitation of our study has to do with relative dynamic ranges of the various in vivo parameters. While we showed that this concern was not applicable to our previously published longitudinal analyses,[26,27] in this study it is possible that a more constrained dynamic range for RNFL thickness change could lead to apparently greater loss (longitudinal change as a percent of baseline values) for RNFL retardance (or retinal function). For example, if the RNFL thickness parameter has a "floor" at approximately 40% of its baseline value,[48,49] then its dynamic range is compressed to only 60%. If the retardance parameter enjoys a dynamic range that is otherwise 100% of its baseline values, the magnitude of relative loss indicated by any given percent decline from baseline will actually be 67% (1/0.6) greater for RNFL thickness as compared to retardance. Adjusting the magnitude of relative loss accordingly for RNFL thickness (i.e., magnifying by 67%) results in shallower slopes for all the linear functions in Figure 2, but it does not alter the *Y*-intercept, which was the basis of our hypothesis test and inference. Applying the same adjustment to account for possible dynamic range compression of RNFL thickness in the comparison to axon loss (Fig. 3A) results in both a shallower slope and a slightly more negative intercept, but one that is still not significantly below zero (−1.3%, 95% CI: −10.2% to +7.7%). Thus, the inferences drawn from the analyses applied in this study appear to be robust even if there is a substantial differential in the relative dynamic range across in vivo parameters. Though few animals in this study were followed to a severe damage stage (and none to end-stage damage; the most severe case had 82.1% axon loss) and thus limited capacity to specifically address the question of relative differences in the "floor" for each parameter, the evidence available in Figure 3 implies that there is not a substantial difference between the dynamic ranges for RNFL thickness and retardance. This is somewhat surprising given that the residual thickness is assumed to consist of glia (e.g., Müller cell endfeet, astrocytes, microglia), capillaries, and the internal limiting membrane, whereas the retardance measurement should extend to zero theoretically once all axons are extinguished. It remains to be determined precisely what contributes to residual values of each measurement. Polarization-sensitive OCT[50–55] and/or second harmonic generation imaging[56,57] may help answer these questions and provide more direct probes of axonal cytoskeletal integrity.

The strengths of this study include the following. (1) The sample size was relatively large and included EG eyes spanning a wide range of damage, as well as a relatively large number of EG eyes with axon counts obtained at an early stage with only minimal to mild damage. (2) Since this EG model is inducible and unilateral, it enabled comparison of EG and fellow control eyes to their own true baseline, healthy state. (3) The method of obtaining complete (100%) axon counts for each optic nerve minimizes the error and risk of underestimation inherent to subsampling strategies (e.g., see Supplementary Fig. S2 in Fortune et al.[19]). Within the context of these issues, it is important to note that a recent clinical study by Xu et al.[58] found that in eyes of human patients with established glaucoma, progression occurred most frequently and generally earlier by RNFL thickness as compared with RNFL retardance. Though that study cohort included many eyes with only mild or moderate visual field loss [76% mild (MD $\geq$ –6 dB), 15% moderate (–6 dB $>$ MD $>$ −12 dB)], RFNL damage was generally more severe as indicated in their Table 2 and Figures 3 and 4.[58] Taken together, the results of the study by Xu et al.[58] and the present study suggest that the differential between RNFL retardance and thickness is most meaningful at the earliest stages of damage. Specific evidence of this is shown in Figure 2A, where 29 of the 31 EG eyes with $<$20% loss of RNFL thickness lie below the 1:1 diagonal; in contrast, eyes with $>$20% RNFL thickness loss straddle the 1:1 diagonal.

In summary, this study provides evidence that both RNFL retardance measured by SLP and RGC function measured by mfERG HFC amplitudes exhibit progressive loss from baseline before any loss of RNFL thickness or orbital optic nerve axons

Investigative Ophthalmology & Visual Science

occurs in NHP EG. Thus both of these in vivo measures might serve as potential biomarkers of early-stage glaucomatous damage, which appears to precede axon loss and RGC death. The aim of future studies is to test whether this early damage stage is reversible with therapeutic intervention.

Acknowledgments

The authors thank Galen Williams, Christy Hardin, and Luke Reyes for their expert technical assistance during data collection and Shaban Demirel for statistical expertise and consultation.

Supported by National Institutes of Health R01-EY019327 (BF), R01-EY011610 (CFB); Legacy Good Samaritan Foundation; Heidelberg Engineering, GmbH, Heidelberg, Germany (equipment and unrestricted research support); Carl Zeiss Meditec, Inc. (equipment).

Disclosure: **B. Fortune**, Heidelberg Engineering, GmbH (F), Carl Zeiss Meditec, Inc. (F); **G. Cull**, None; **J. Reynaud**, None; **L. Wang**, None; **C.F. Burgoyne**, Heidelberg Engineering, GmbH (F, C, R)

References

1. Hoyt WF, Newman NM. The earliest observable defect in glaucoma? *Lancet*. 1972;1:692–693.
2. Hoyt WF, Frisen L, Newman NM. Fundoscopy of nerve fiber layer defects in glaucoma. *Invest Ophthalmol*. 1973;12:814–829.
3. Sommer A, Katz J, Quigley HA, et al. Clinically detectable nerve fiber atrophy precedes the onset of glaucomatous field loss. *Arch Ophthalmol*. 1991;109:77–83.
4. Quigley HA, Addicks EM. Quantitative studies of retinal nerve fiber layer defects. *Arch Ophthalmol*. 1982;100:807–814.
5. Quigley HA. Examination of the retinal nerve fiber layer in the recognition of early glaucoma damage. *Trans Am Ophthalmol Soc*. 1986;84:920–966.
6. Weinreb RN, Dreher AW, Coleman A, Quigley H, Shaw B, Reiter K. Histopathologic validation of Fourier-ellipsometry measurements of retinal nerve fiber layer thickness. *Arch Ophthalmol*. 1990;108:557–560.
7. Huang XR, Knighton RW. Linear birefringence of the retinal nerve fiber layer measured in vitro with a multispectral imaging micropolarimeter. *J Biomed Opt*. 2002;7:199–204.
8. Huang D, Swanson EA, Lin CP, et al. Optical coherence tomography. *Science*. 1991;254:1178–1181.
9. Zangwill LM, Bowd C. Retinal nerve fiber layer analysis in the diagnosis of glaucoma. *Curr Opin Ophthalmol*. 2006;17:120–131.
10. Townsend KA, Wollstein G, Schuman JS. Imaging of the retinal nerve fibre layer for glaucoma. *Br J Ophthalmol*. 2009;93:139–143.
11. Leung CK. Diagnosing glaucoma progression with optical coherence tomography. *Curr Opin Ophthalmol*. 2014;25:104–111.
12. Kawaguchi I, Higashide T, Ohkubo S, Takeda H, Sugiyama K. In vivo imaging and quantitative evaluation of the rat retinal nerve fiber layer using scanning laser ophthalmoscopy. *Invest Ophthalmol Vis Sci*. 2006;47:2911–2916.
13. Nagata A, Higashide T, Ohkubo S, Takeda H, Sugiyama K. In vivo quantitative evaluation of the rat retinal nerve fiber layer with optical coherence tomography. *Invest Ophthalmol Vis Sci*. 2009;50:2809–2815.
14. Schuman JS, Pedut-Kloizman T, Pakter H, et al. Optical coherence tomography and histologic measurements of nerve fiber layer thickness in normal and glaucomatous monkey eyes. *Invest Ophthalmol Vis Sci*. 2007;48:3645–3654.
15. Chauhan BC, Stevens KT, Levesque JM, et al. Longitudinal in vivo imaging of retinal ganglion cells and retinal thickness changes following optic nerve injury in mice. *PLoS One*. 2012;7:e40352.
16. Choe TE, Abbott CJ, Piper C, Wang L, Fortune B. Comparison of longitudinal in vivo measurements of retinal nerve fiber layer thickness and retinal ganglion cell density after optic nerve transection in rat. *PLoS One*. 2014;9:e113011.
17. Gabelt BT, Rasmussen CA, Tektas OY, et al. Structure/function studies and the effects of memantine in monkeys with experimental glaucoma. *Invest Ophthalmol Vis Sci*. 2012;53:2368–2376.
18. Cull GA, Reynaud J, Wang L, Cioffi GA, Burgoyne CF, Fortune B. Relationship between orbital optic nerve axon counts and retinal nerve fiber layer thickness measured by spectral domain optical coherence tomography. *Invest Ophthalmol Vis Sci*. 2012;53:7766–7773.
19. Fortune B, Reynaud J, Cull G, Burgoyne CF, Wang L. The effect of age on optic nerve axon counts, SDOCT scan quality, and peripapillary retinal nerve fiber layer thickness measurements in rhesus monkeys. *Trans Vis Sci Technol*. 2014;3:2.
20. Zhou Q, Knighton RW. Light scattering and form birefringence of parallel cylindrical arrays that represent cellular organelles of the retinal nerve fiber layer. *Appl Opt*. 1997;36:2273–2285.
21. Huang XR, Bagga H, Greenfield DS, Knighton RW. Variation of peripapillary retinal nerve fiber layer birefringence in normal human subjects. *Invest Ophthalmol Vis Sci*. 2004;45:3073–3080.
22. Huang XR, Knighton RW. Microtubules contribute to the birefringence of the retinal nerve fiber layer. *Invest Ophthalmol Vis Sci*. 2005;46:4588–4593.
23. Fortune B, Wang L, Cull G, Cioffi GA. Intravitreal colchicine causes decreased RNFL birefringence without altering RNFL thickness. *Invest Ophthalmol Vis Sci*. 2008;49:255–261.
24. Pocock GM, Aranibar RG, Kemp NJ, Specht CS, Markey MK, Rylander HG III. The relationship between retinal ganglion cell axon constituents and retinal nerve fiber layer birefringence in the primate. *Invest Ophthalmol Vis Sci*. 2009;50:5238–5246.
25. Fortune B, Cull GA, Burgoyne CF. Relative course of retinal nerve fiber layer birefringence and thickness and retinal function changes after optic nerve transection. *Invest Ophthalmol Vis Sci*. 2008;49:4444–4452.
26. Fortune B, Burgoyne CF, Cull GA, Reynaud J, Wang L. Structural and functional abnormalities of retinal ganglion cells measured in vivo at the onset of optic nerve head surface change in experimental glaucoma. *Invest Ophthalmol Vis Sci*. 2012;53:3939–3950.
27. Fortune B, Burgoyne CF, Cull G, Reynaud J, Wang L. Onset and progression of peripapillary retinal nerve fiber layer (RNFL) retardance changes occur earlier than RNFL thickness changes in experimental glaucoma. *Invest Ophthalmol Vis Sci*. 2013;54:5653–5661.
28. Fortune B, Reynaud J, Wang L, Burgoyne CF. Does optic nerve head surface topography change prior to loss of retinal nerve fiber layer thickness: a test of the site of injury hypothesis in experimental glaucoma. *PLoS One*. 2013;8:e77831.
29. Fortune B, Yang H, Strouthidis NG, et al. The effect of acute intraocular pressure elevation on peripapillary retinal thickness, retinal nerve fiber layer thickness, and retardance. *Invest Ophthalmol Vis Sci*. 2009;50:4719–4726.
30. Laser Diagnostic Technologies, Inc. *RNFL Analysis with GDxVCC: A Primer and Clinical Guide*. San Diego, CA: Laser Diagnostic Technologies, Inc.; 2004:14.a.
31. Fortune B, Wang L, Bui BV, Cull G, Dong J, Cioffi GA. Local ganglion cell contributions to the macaque electroretinogram revealed by experimental nerve fiber layer bundle defect. *Invest Ophthalmol Vis Sci*. 2003;44:4567–4579.

32. Fortune B, Wang L, Bui BV, Burgoyne CF, Cioffi GA. Idiopathic bilateral optic atrophy in the rhesus macaque. *Invest Ophthalmol Vis Sci*. 2005;46:3943–3956.
33. Gaasterland D, Kupfer C. Experimental glaucoma in the rhesus monkey. *Invest Ophthalmol*. 1974;13:455–457.
34. Quigley HA, Hohman RM. Laser energy levels for trabecular meshwork damage in the primate eye. *Invest Ophthalmol Vis Sci*. 1983;24:1305–1307.
35. Reynaud J, Cull G, Wang L, et al. Automated quantification of optic nerve axons in primate glaucomatous and normal eyes–method and comparison to semi-automated manual quantification. *Invest Ophthalmol Vis Sci*. 2012;53:2951–2959.
36. Cull GA, Reynaud J, Wang L, Cioffi GA, Burgoyne CF, Fortune B. Erratum in: "Relationship Between Orbital Optic Nerve Axon Counts and Retinal Nerve Fiber Layer Thickness Measured by Spectral Domain Optical Coherence Tomography." *Invest Ophthalmol Vis Sci*. 2014;55:2619–2620.
37. Luo X, Patel NB, Rajagopalan LP, Harwerth RS, Frishman LJ. Relation between macular retinal ganglion cell/inner plexiform layer thickness and multifocal electroretinogram measures in experimental glaucoma. *Invest Ophthalmol Vis Sci*. 2014;55:4512–4524.
38. Viswanathan S, Frishman LJ, Robson JG, Harwerth RS, Smith EL III. The photopic negative response of the macaque electroretinogram: reduction by experimental glaucoma. *Invest Ophthalmol Vis Sci*. 1999;40:1124–1136.
39. Viswanathan S, Frishman LJ, Robson JG, Walters JW. The photopic negative response of the flash electroretinogram in primary open angle glaucoma. *Invest Ophthalmol Vis Sci*. 2001;42:514–522.
40. Colotto A, Falsini B, Salgarello T, Iarossi G, Galan ME, Scullica L. Photopic negative response of the human ERG: losses associated with glaucomatous damage. *Invest Ophthalmol Vis Sci*. 2000;41:2205–2211.
41. Rangaswamy NV, Frishman LJ, Dorotheo EU, Schiffman JS, Bahrani HM, Tang RA. Photopic ERGs in patients with optic neuropathies: comparison with primate ERGs after pharmacologic blockade of inner retina. *Invest Ophthalmol Vis Sci*. 2004;45:3827–3837.
42. Chrysostomou V, Crowston JG. The photopic negative response of the mouse electroretinogram: reduction by acute elevation of intraocular pressure. *Invest Ophthalmol Vis Sci*. 2013;54:4691–4697.
43. Strouthidis NG, Fortune B, Yang H, Sigal IA, Burgoyne CF. Longitudinal change detected by spectral domain optical coherence tomography in the optic nerve head and peripapillary retina in experimental glaucoma. *Invest Ophthalmol Vis Sci*. 2011;52:1206–1219.
44. He L, Yang H, Gardiner SK, et al. Longitudinal detection of optic nerve head changes by spectral domain optical coherence tomography in early experimental glaucoma. *Invest Ophthalmol Vis Sci*. 2014;55:574–586.
45. Yang H, He L, Gardiner SK, et al. Age-related differences in longitudinal structural change by spectral-domain optical coherence tomography in early experimental glaucoma. *Invest Ophthalmol Vis Sci*. 2014;55:6409–6420.
46. de Lima S, Koriyama Y, Kurimoto T, et al. Full-length axon regeneration in the adult mouse optic nerve and partial recovery of simple visual behaviors. *Proc Natl Acad Sci U S A*. 2012;109:9149–9154.
47. Rangaswamy NV, Zhou W, Harwerth RS, Frishman LJ. Effect of experimental glaucoma in primates on oscillatory potentials of the slow-sequence mfERG. *Invest Ophthalmol Vis Sci*. 2006;47:753–767.
48. Sihota R, Sony P, Gupta V, Dada T, Singh R. Diagnostic capability of optical coherence tomography in evaluating the degree of glaucomatous retinal nerve fiber damage. *Invest Ophthalmol Vis Sci*. 2006;47:2006–2010.
49. Chan CK, Miller NR. Peripapillary nerve fiber layer thickness measured by optical coherence tomography in patients with no light perception from long-standing nonglaucomatous optic neuropathies. *J Neuroophthalmol*. 2007;27:176–179.
50. Cense B, Chen TC, Park BH, Pierce MC, de Boer JF. Invivo depth-resolved birefringence measurements of the human retinal nerve fiber layer by polarization-sensitive optical coherence tomography. *Opt Lett*. 2002;27:1610–1612.
51. Cense B, Chen TC, Park BH, Pierce MC, de Boer JF. Thickness and birefringence of healthy retinal nerve fiber layer tissue measured with polarization-sensitive optical coherence tomography. *Invest Ophthalmol Vis Sci*. 2004;45:2606–2612.
52. Cense B, Chen TC, Park BH, Pierce MC, de Boer JF. In vivo birefringence and thickness measurements of the human retinal nerve fiber layer using polarization-sensitive optical coherence tomography. *J Biomed Opt*. 2004;9:121–125.
53. Pircher M, Hitzenberger CK, Schmidt-Erfurth U. Polarization sensitive optical coherence tomography in the human eye. *Prog Retin Eye Res*. 2011;30:431–451.
54. Zotter S, Pircher M, Gotzinger E, et al. Measuring retinal nerve fiber layer birefringence, retardation, and thickness using wide-field, high-speed polarization sensitive spectral domain OCT. *Invest Ophthalmol Vis Sci*. 2013;54:72–84.
55. Braaf B, Vermeer KA, de Groot M, Vienola KV, de Boer JF. Fiber-based polarization-sensitive OCT of the human retina with correction of system polarization distortions. *Biomed Opt Express*. 2014;5:2736–2758.
56. Lim H, Danias J. Label-free morphometry of retinal nerve fiber bundles by second-harmonic-generation microscopy. *Opt Lett*. 2012;37:2316–2318.
57. Lim H, Danias J. Effect of axonal micro-tubules on the morphology of retinal nerve fibers studied by second-harmonic generation. *J Biomed Opt*. 2012;17:110502.
58. Xu G, Weinreb RN, Leung CK. Retinal nerve fiber layer progression in glaucoma: a comparison between retinal nerve fiber layer thickness and retardance. *Ophthalmology*. 2013;120:2493–2500.

Investigative Ophthalmology & Visual Science